

DOI: 10.7511/jslx20230104001

压电材料切口奇异物理场计算

潘伟, 程长征*, 王飞杨, 李腾岳, 牛忠荣

(合肥工业大学 土木与水利工程学院, 合肥 230009)

摘要:采用切口尖端奇性特征分析与有限元法相结合的思路, 计算压电材料切口尖端的力学和电学奇异物理场。首先基于奇性渐近展开技巧, 推演压电材料切口的奇性特征方程, 引入插值矩阵法求解, 获得切口尖端奇性渐近展开式的奇性指数、特征角函数及其导数。再根据有限元法的位移和电势计算结果较应力和电位移高一阶精度的特点, 利用稀疏有限元网格, 计算出切口附近的位移和电势, 代入切口尖端物理场渐近展开式, 求出幅值系数。根据计算出的幅值系数、奇性指数、特征角函数及其导数, 重构出切口尖端附近的奇异应力场和电位移场, 继而计算出切口的应力强度因子和电位移强度因子。本文提出半解析方法, 基于有限元稀疏网格计算结果, 利用较小的计算量, 获得较高精度的奇异物理场。该方法无须对有限元法的插值函数进行改造, 适合嵌入商业有限元软件, 直接用于工程压电材料结构安全分析。

关键词:压电材料; 切口; 渐近展开; 奇异应力场; 奇异电位移场

中图分类号: O343

文献标志码: A

文章编号: 1007-4708(2024)04-0742-07

1 引言

压电材料具有将机械能和电能进行相互转化的特性, 常用作执行器和传感器等元器件。在制造和使用过程中, 压电材料结构会产生孔洞和切口甚至裂纹等缺陷。切口尖端的奇异应力或奇异电位移会使压电材料结构产生强度破坏或电荷击穿。切口尖端的奇异物理场计算, 对评估压电材料结构安全和保持压电元器件性能稳定具有重要的作用。

裂纹作为切口张角为零度的特例, 其尖端的奇异性也是所有切口中最强的, 压电材料裂纹尖端的奇异性首先引起了学者的关注^[1-4]。切口尖端的奇异性虽然较裂纹弱一些, 但由于其奇异性不是负的1/2, 分析起来要复杂得多。Hirai等^[5]结合Stroh形式和Williams特征函数展开方法, 得到了压电双材料界面角附近的渐近解。Hrstka等^[6]使用扩展的Lekhnitskii-Eshelby-Stroh形式, 研究了压电双材料尖锐切口的平面问题。程长征等^[7]基于顶点附近物理场渐近展开, 研究了磁电弹材料切口的奇异特征。周震寰等^[8]在哈密顿力学框架下, 研究

了一维六方准晶双材料中的III型界面V形切口。平学成等^[9]建立了分析压电材料切口端部奇异弹性场的杂交有限元法。目前的研究主要集中在压电材料切口的奇性特征分析, 少量的压电切口尖端奇异场分析方法需要构造特殊的奇异单元, 对推广到多材料切口奇异物理场问题有困难。

本文提出一种切口奇性特征分析与有限元法相结合的方法, 计算压电材料切口尖端奇异物理场。首先, 采用奇性渐近展开技巧, 将切口尖端位移和电势进行渐近展开, 通过特征分析, 获得奇性指数、特征角函数及其导数。再利用稀疏有限元网格, 对压电材料结构进行有限元分析, 获取切口尖端附近的位移和电势。随后, 将有限元计算结果代入奇性渐近展开表达式, 求解出渐近展开式的幅值系数。最后, 依据求得的幅值系数、奇性指数和特征角函数及其导数, 重构出切口尖端的奇异应力场和奇异电位移场, 同时计算出切口的应力强度因子和电位移强度因子。

2 压电材料切口尖端奇性特征分析

考虑如图1(a)所示的压电材料切口结构, 切

收稿日期: 2023-01-04; 修改稿收到日期: 2023-02-12.

基金项目: 国家自然科学基金(12172114); 安徽省杰出青年自然科学基金(2208085J25)资助项目。

作者简介: 程长征*(1979-), 男, 博士, 教授, 博士生导师(E-mail: changzheng_cheng@hfut.edu.cn).

引用本文: 潘伟, 程长征, 王飞杨, 等. 压电材料切口奇异物理场计算[J]. 计算力学学报, 2024, 41(4): 742-748.

PAN Wei, CHENG Chang-zheng, WANG Fei-yang, et al. Evaluation of singular physical field near the vertex of piezoelectric material notch[J]. Chinese Journal of Computational Mechanics, 2024, 41(4): 742-748.

口尖端为应力和电位移奇异区域,将切口尖端的扇形区域提取出来单独分析,如图 1(b)所示,图中 ox_1x_2 为原点在电弹性场奇异点的整体直角坐标系, $ox'_1x'_2$ 为材料的极化轴, $o\rho\theta$ 为极坐标系, φ 为切口张角, β 为极化方向与 x_2 轴的夹角。在直角坐标系 ox_1x_2 下,压电材料的线性本构方程为

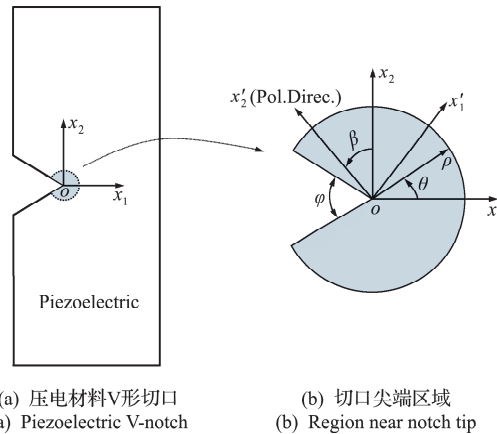


图 1 压电材料 V 形切口及切口尖端区域
Fig. 1 A piezoelectric V-notch and region near notch tip

$$\{\sigma\} = [C]\{\epsilon\} - [e]^T\{E\} \quad (1a)$$

$$\{D\} = [e]\{\epsilon\} - [\kappa]\{E\} \quad (1b)$$

式中 $\{\sigma\}$ 和 $\{D\}$ 分别为应力张量和电位移矢量, $\{\epsilon\}$ 为应变张量, $\{E\}$ 为电场矢量, $[C]$ 和 $[e]$ 分别为弹性常数和压电常数, $[\kappa]$ 为介电常数。

经过坐标变换,可得极坐标系下的应力和电位移表达式为

$$\{X_i\} = \left\{ Q_{i1} \frac{\partial u_\rho}{\partial \rho} + Q_{i2} \left(\frac{u_\rho}{\rho} + \frac{1}{\rho} \frac{\partial u_\theta}{\partial \theta} \right) + Q_{i3} \left(\frac{1}{\rho} \frac{\partial u_\rho}{\partial \theta} + \frac{\partial u_\theta}{\partial \rho} - \frac{u_\theta}{\rho} \right) - Q_{i4} \frac{\partial \phi}{\partial \rho} - Q_{i5} \frac{1}{\rho} \frac{\partial \phi}{\partial \theta} \right\} \quad (2)$$

式中 $\{X_i\}$ ($i=1, \dots, 5$) 依次为 (ρ, θ) 处的径向正应力 σ_ρ 、切向正应力 σ_θ 、切应力 $\sigma_{\rho\theta}$ 以及径向电位移 D_ρ 、切向电位移 D_θ ; u_ρ, u_θ 和 ϕ 分别是 (ρ, θ) 处的径向位移、环向位移和电势,系数 Q_{ij} ($i, j=1, \dots, 5$) 是压电材料参数 $[C], [e]$ 和 $[\kappa]$ 与极化角度 $(\theta - \beta)$ 的三角函数的乘积。

按渐近展开理论,切口尖端附近的位移场和电势场可表示为^[10]

$$\begin{cases} u_\rho(\rho, \theta) = \sum_{k=1}^N A_k \rho^{\lambda_k+1} \bar{u}_{\rho k}(\lambda_k, \theta) \\ u_\theta(\rho, \theta) = \sum_{k=1}^N A_k \rho^{\lambda_k+1} \bar{u}_{\theta k}(\lambda_k, \theta) \\ \phi(\rho, \theta) = \sum_{k=1}^N A_k \rho^{\lambda_k+1} \tilde{\phi}_k(\lambda_k, \theta) \end{cases} \quad (3)$$

式中 A_k 为渐近展开级数的幅值系数, λ_k 为应力和电位移奇性指数, $\bar{u}_{\rho k}(\lambda_k, \theta), \bar{u}_{\theta k}(\lambda_k, \theta)$ 和 $\tilde{\phi}_k(\lambda_k, \theta)$ 为位移和电势特征角函数。

将式(3)代入式(2),再代入到压电材料的静力学平衡方程和 Maxwell 方程,可以得到压电材料切口奇性特征方程

$$\begin{aligned} & Q_{33} \bar{u}_r'' + Q_{32} \bar{u}_\theta'' - Q_{35} \tilde{\phi}'' + (Q_{32} - Q_{23} + Q'_{33}) \bar{u}_r' + \\ & (Q'_{32} - Q_{22} - Q_{33}) \bar{u}_\theta' + (Q_{25} - Q'_{35}) \tilde{\phi}' + \\ & (Q'_{32} - Q_{22}) \bar{u}_r + (Q_{23} - Q'_{33}) \bar{u}_\theta + \\ & \lambda(Q_{31} + Q_{13}) \bar{u}_r' + \lambda(Q_{12} + Q_{33}) \bar{u}_\theta' - \\ & \lambda(Q_{15} + Q_{34}) \tilde{\phi}' + \lambda^2 Q_{11} \bar{u}_r + \lambda^2 Q_{13} \bar{u}_\theta - \\ & \lambda^2 Q_{14} \tilde{\phi} + \lambda(Q_{12} - Q_{21} + Q'_{31}) \bar{u}_r + \\ & \lambda(Q'_{33} - Q_{13} - Q_{23}) \bar{u}_\theta + \lambda(Q_{24} - Q'_{34}) \tilde{\phi} = 0 \quad (4a) \end{aligned}$$

$$\begin{aligned} & Q_{23} \bar{u}_r'' + Q_{22} \bar{u}_\theta'' - Q_{25} \tilde{\phi}'' + (Q_{22} + Q_{33} + Q'_{23}) \bar{u}_r' + \\ & (Q_{32} - Q_{23} + Q'_{22}) \bar{u}_\theta' - (Q_{35} + Q'_{25}) \tilde{\phi}' + \\ & (Q_{32} + Q'_{22}) \bar{u}_r - (Q_{33} + Q'_{23}) \bar{u}_\theta + \\ & \lambda(Q_{21} + Q_{33}) \bar{u}_r' + \lambda(Q_{23} + Q_{32}) \bar{u}_\theta' - \\ & \lambda(Q_{24} + Q_{35}) \tilde{\phi}' + \lambda^2 Q_{31} \bar{u}_r + \lambda^2 Q_{33} \bar{u}_\theta - \\ & \lambda^2 Q_{34} \tilde{\phi} + \lambda(Q'_{21} + Q_{32} + Q_{31}) \bar{u}_r + \\ & \lambda Q'_{23} \bar{u}_\theta - \lambda(Q'_{24} + Q_{34}) \tilde{\phi} = 0 \quad (4b) \end{aligned}$$

$$\begin{aligned} & Q_{53} \bar{u}_r'' + Q_{52} \bar{u}_\theta'' - Q_{55} \tilde{\phi}'' + (Q_{52} + Q'_{53}) \bar{u}_r' + \\ & (Q'_{52} - Q_{53}) \bar{u}_\theta' - Q'_{55} \tilde{\phi}' + Q'_{52} \bar{u}_r - Q'_{53} \bar{u}_\theta + \\ & \lambda(Q_{43} + Q_{51}) \bar{u}_r' + \lambda(Q_{42} + Q_{53}) \bar{u}_\theta' - \\ & \lambda(Q_{45} + Q_{54}) \tilde{\phi}' + \lambda^2 Q_{41} \bar{u}_r + \lambda^2 Q_{43} \bar{u}_\theta - \\ & \lambda^2 Q_{44} \tilde{\phi} + \lambda(Q_{42} + Q'_{51}) \bar{u}_r + \\ & \lambda(Q'_{53} - Q_{43}) \bar{u}_\theta - \lambda Q'_{54} \tilde{\phi} = 0 \quad (4c) \end{aligned}$$

式中 $(\cdots)' = d(\cdots)/d\theta, (\cdots)'' = d^2(\cdots)/d\theta^2$ 。引入切口径向边界上表面力和电位移边界条件后,可以通过牛忠荣等^[11]提出的插值矩阵法求解上述特征方程组,得到切口奇性指数 λ_k 和特征角函数 $\bar{u}_{\rho k}, \bar{u}_{\theta k}$ 和 $\tilde{\phi}_k$, 以及特征角函数的一阶和二阶导数。

3 压电材料切口渐近展开式幅值系数计算

本节研究计算压电材料切口尖端物理场渐近展开式(3)的幅值系数 A_k 。采用有限元法对含切口结构进行单元离散,如图 2(a)所示。在切口尖端采用稀疏网格,如图 2(b)所示,经有限元计算,获得单元节点的位移和电势。为了获得参考解,将原来的稀疏网格在径向和环向上加密后得到精细化网格,如图 2(c)所示。考虑到有限元结果一般是在直角坐标系下给出,将式(3)变化到直角坐标系下,可表示为

$$\begin{bmatrix} \cos\theta & \sin\theta & 0 \\ -\sin\theta & \cos\theta & 0 \\ 0 & 0 & 1 \end{bmatrix} \begin{bmatrix} u_1 \\ u_2 \\ \phi \end{bmatrix} = \begin{bmatrix} \sum_{k=1}^N A_k \rho^{\lambda_k+1} \tilde{u}_{\rho k}(\theta) \\ \sum_{k=1}^N A_k \rho^{\lambda_k+1} \tilde{u}_{\theta k}(\theta) \\ \sum_{k=1}^N A_k \rho^{\lambda_k+1} \tilde{\phi}_k(\theta) \end{bmatrix} \quad (5)$$

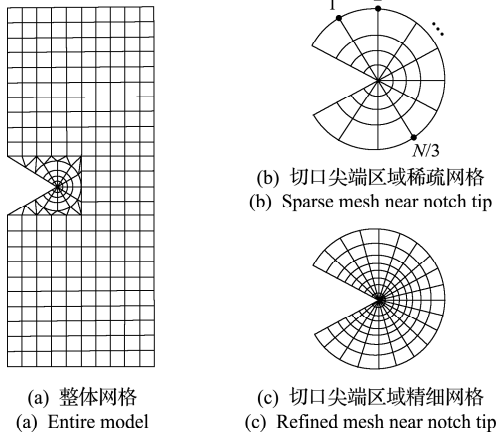


图 2 有限元分析网格
Fig. 2 Finite element method mesh

假设截取渐近展开式前 N 项, 这样共有 N 个待求系数 $A_k (k=1, 2, \dots, N)$ 。如图 2(b) 所示, 在有限元网格上选 $N/3$ 个节点, 其坐标为 $(\rho_i, \theta_i) (i=1, 2, \dots, N/3)$ 。取出计算得到的每个点的 u_1, u_2 和 ϕ 值, 代入式(5), 每个点列 3 个方程, $N/3$ 个点共可以得到含 N 个方程的正定方程组, 从中可求解出所有的幅值系数 $A_k (k=1, 2, \dots, N)$ 。

然后, 将式(3)引入式(2), 得到切口尖端的奇异应力场和电位移场为

$$X_i(\rho, \theta) = \sum_{k=1}^N A_k \rho^{\lambda_k} \left\{ [(\lambda_k + 1)Q_{i1} + Q_{i2}] \tilde{u}_{\rho k} + Q_{i3} \tilde{u}'_{\rho k} + \lambda_k Q_{i3} \tilde{u}_{\theta k} + Q_{i2} \tilde{u}'_{\theta k} - (\lambda_k + 1)Q_{i4} \tilde{\phi}_k - Q_{i5} \tilde{\phi}'_k \right\} \quad (6)$$

因此, 在获得幅值系数 A_k 后, 基于奇性分析计算得到的奇性指数 λ_k 和特征角函数 $\tilde{u}_{\rho k}, \tilde{u}_{\theta k}, \tilde{\phi}_k$ 以及其导数 $\tilde{u}'_{\rho k}, \tilde{u}'_{\theta k}$ 和 $\tilde{\phi}'_k$, 可以计算出切口尖端附近的奇异应力场和奇异电位移场。

利用幅值系数 A_k 和特征角函数, 按式(7)^[12] 可计算出 V 形切口的应力强度因子和电位移强度因子。

$$K_1 = \lim_{\rho \rightarrow 0} \sqrt{2\pi} \rho^{-\lambda_1} \sigma_\theta(\rho, \theta) |_{\theta=0} = \sqrt{2\pi} A_1 \left\{ [(\lambda_1 + 1)Q_{21} + Q_{22}] \tilde{u}_{\rho 1} + Q_{23} \tilde{u}'_{\rho 1} + \lambda_1 Q_{23} \tilde{u}_{\theta 1} + Q_{22} \tilde{u}'_{\theta 1} - (\lambda_1 + 1)Q_{24} \tilde{\phi}_1 - Q_{25} \tilde{\phi}'_1 \right\} |_{\theta=0} \quad (7a)$$

$$K_D = \lim_{\rho \rightarrow 0} \sqrt{2\pi} \rho^{-\lambda_D} D_\theta(\rho, \theta) |_{\theta=0} = \sqrt{2\pi} A_D \left\{ [(\lambda_D + 1)Q_{51} + Q_{52}] \tilde{u}_{\rho D} + Q_{53} \tilde{u}'_{\rho D} + \lambda_D Q_{53} \tilde{u}_{\theta D} + Q_{52} \tilde{u}'_{\theta D} - (\lambda_D + 1)Q_{54} \tilde{\phi}_D - Q_{55} \tilde{\phi}'_D \right\} |_{\theta=0} \quad (7b)$$

4 数值算例

首先, 利用插值矩阵法求解特征方程组(4), 获得压电材料切口的奇性指数和特征角函数, 然后利用稀疏单元划分的有限元法对含切口压电材料结构进行分析, 获得切口尖端区域内点的位移和电势值, 通过方程(5)解得幅值系数。最后, 通过式(6)重构切口尖端奇异应力和奇异电位移, 通过式(7)计算切口的力学和电学强度因子。

4.1 压电材料切口的奇性指数和特征角函数

本文以 PZT-4 压电材料为例, 其材料性能参数见文献[13]。首先, 计算 PZT-4 压电材料切口的奇性指数 λ_k 和特征角函数。图 3 给出了极化方向沿 x_2 轴时 λ_k 随切口角 φ 的变化, 并与文献[13]采用复势函数法分析结果比较, 可以看出, 本文结果与参考解吻合较好。图 4 给出了当切口张角 $\varphi = 60^\circ$ 时, 压电材料切口的第一阶奇性指数对应的特征角函数及其一阶导数。

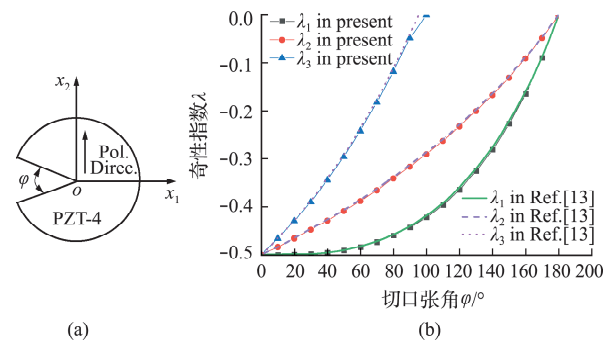


图 3 PZT-4 切口奇性指数随切口张角的变化
Fig. 3 Variation of singularity orders with φ for PZT-4 notch

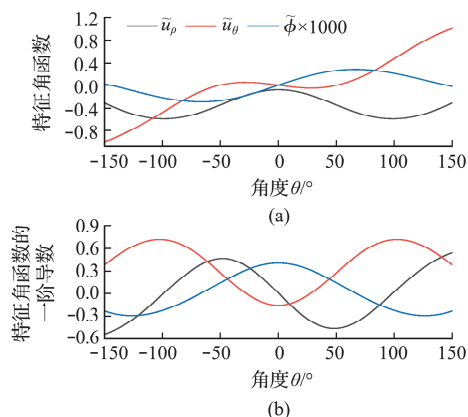


图 4 $\varphi = 60^\circ$ 切口的第一阶特征角函数及其一阶导数
Fig. 4 Characteristic angular functions and its first derivatives for PZT-4 notch when $\varphi = 60^\circ$

4.2 压电材料切口的幅值系数和强度因子

考虑如图 5 所示 PZT-4 切口板,切口张角 $\varphi=60^\circ$,板宽 $W=3$ mm,板长 $L=15$ mm,切口深度 $d=1$ mm,极化方向平行于 x_2 轴,受到均匀的张力 $\sigma_{22}^0=5$ MPa 和电位移 $D_2^0=0.1$ C/m² 作用。

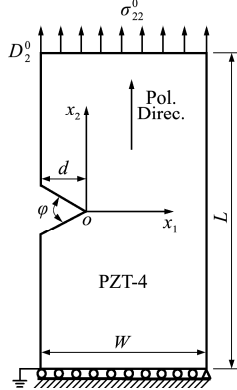


Fig. 5 A tensile PZT-4 notched plate

如图 6(a)所示,分别取切口径向边界 Γ_1 和 Γ_3 上的一点,以及切口对角线上的一点,这 3 个点与切口尖端之间的距离分别为 ρ_{Γ_i} ($i=1,2,3$),其 θ 坐标分别记为 θ_i ($i=1,2,3$)。将这 3 个点的位移有限元法计算结果以及奇性特征分析计算得到的 λ_k , $\bar{u}_{\rho k}$ 和 $\bar{u}_{\theta k}$ 代入式(5),得到一个 6 阶的方程组为

$$\begin{bmatrix} \rho_{\Gamma_1}^{\lambda_1+1} \bar{u}_{\rho 1}^{\Gamma_1} & \rho_{\Gamma_1}^{\lambda_2+1} \bar{u}_{\rho 2}^{\Gamma_1} & \cdots & \rho_{\Gamma_1}^{\lambda_6+1} \bar{u}_{\rho 6}^{\Gamma_1} \\ \rho_{\Gamma_1}^{\lambda_1+1} \bar{u}_{\theta 1}^{\Gamma_1} & \rho_{\Gamma_1}^{\lambda_2+1} \bar{u}_{\theta 2}^{\Gamma_1} & \cdots & \rho_{\Gamma_1}^{\lambda_6+1} \bar{u}_{\theta 6}^{\Gamma_1} \\ \rho_{\Gamma_2}^{\lambda_1+1} \bar{u}_{\rho 1}^{\Gamma_2} & \rho_{\Gamma_2}^{\lambda_2+1} \bar{u}_{\rho 2}^{\Gamma_2} & \cdots & \rho_{\Gamma_2}^{\lambda_6+1} \bar{u}_{\rho 6}^{\Gamma_2} \\ \rho_{\Gamma_2}^{\lambda_1+1} \bar{u}_{\theta 1}^{\Gamma_2} & \rho_{\Gamma_2}^{\lambda_2+1} \bar{u}_{\theta 2}^{\Gamma_2} & \cdots & \rho_{\Gamma_2}^{\lambda_6+1} \bar{u}_{\theta 6}^{\Gamma_2} \\ \rho_{\Gamma_3}^{\lambda_1+1} \bar{u}_{\rho 1}^{\Gamma_3} & \rho_{\Gamma_3}^{\lambda_2+1} \bar{u}_{\rho 2}^{\Gamma_3} & \cdots & \rho_{\Gamma_3}^{\lambda_6+1} \bar{u}_{\rho 6}^{\Gamma_3} \\ \rho_{\Gamma_3}^{\lambda_1+1} \bar{u}_{\theta 1}^{\Gamma_3} & \rho_{\Gamma_3}^{\lambda_2+1} \bar{u}_{\theta 2}^{\Gamma_3} & \cdots & \rho_{\Gamma_3}^{\lambda_6+1} \bar{u}_{\theta 6}^{\Gamma_3} \end{bmatrix} = \begin{bmatrix} A_1 \\ A_2 \\ A_3 \\ A_4 \\ A_5 \\ A_6 \end{bmatrix} = \begin{bmatrix} \phi^{\Gamma_1} \\ \phi^{\Gamma_2} \\ \phi^{\Gamma_3} \\ \phi^{\Gamma_4} \\ \phi^{\Gamma_5} \\ \phi^{\Gamma_6} \end{bmatrix} \quad (8a)$$

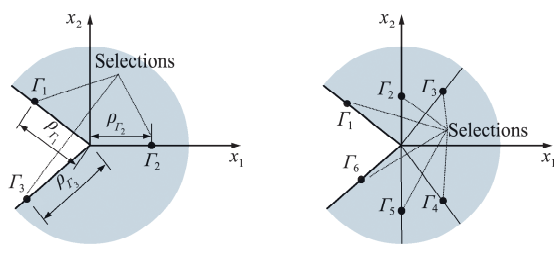


Fig. 6 切口尖端附近计算节点选择
(a) Displacement values of 3 points (b) Potential values of 6 points

Fig. 6 Selections of nodes near the notch tip

也可以用有限元法计算得到的电势来求解渐近展开式的幅值系数。如图 6(b)所示,选取 6 个点的电势值代入式(5),同样得到一个 6 阶的方程组为

$$\begin{bmatrix} \rho_{\Gamma_1}^{\lambda_1+1} \tilde{\phi}_{\Gamma_1}^{\Gamma_1} & \rho_{\Gamma_1}^{\lambda_2+1} \tilde{\phi}_{\Gamma_2}^{\Gamma_1} & \cdots & \rho_{\Gamma_1}^{\lambda_6+1} \tilde{\phi}_{\Gamma_6}^{\Gamma_1} \\ \rho_{\Gamma_2}^{\lambda_1+1} \tilde{\phi}_{\Gamma_1}^{\Gamma_2} & \rho_{\Gamma_2}^{\lambda_2+1} \tilde{\phi}_{\Gamma_2}^{\Gamma_2} & \cdots & \rho_{\Gamma_2}^{\lambda_6+1} \tilde{\phi}_{\Gamma_6}^{\Gamma_2} \\ \rho_{\Gamma_3}^{\lambda_1+1} \tilde{\phi}_{\Gamma_1}^{\Gamma_3} & \rho_{\Gamma_3}^{\lambda_2+1} \tilde{\phi}_{\Gamma_2}^{\Gamma_3} & \cdots & \rho_{\Gamma_3}^{\lambda_6+1} \tilde{\phi}_{\Gamma_6}^{\Gamma_3} \\ \rho_{\Gamma_4}^{\lambda_1+1} \tilde{\phi}_{\Gamma_1}^{\Gamma_4} & \rho_{\Gamma_4}^{\lambda_2+1} \tilde{\phi}_{\Gamma_2}^{\Gamma_4} & \cdots & \rho_{\Gamma_4}^{\lambda_6+1} \tilde{\phi}_{\Gamma_6}^{\Gamma_4} \\ \rho_{\Gamma_5}^{\lambda_1+1} \tilde{\phi}_{\Gamma_1}^{\Gamma_5} & \rho_{\Gamma_5}^{\lambda_2+1} \tilde{\phi}_{\Gamma_2}^{\Gamma_5} & \cdots & \rho_{\Gamma_5}^{\lambda_6+1} \tilde{\phi}_{\Gamma_6}^{\Gamma_5} \\ \rho_{\Gamma_6}^{\lambda_1+1} \tilde{\phi}_{\Gamma_1}^{\Gamma_6} & \rho_{\Gamma_6}^{\lambda_2+1} \tilde{\phi}_{\Gamma_2}^{\Gamma_6} & \cdots & \rho_{\Gamma_6}^{\lambda_6+1} \tilde{\phi}_{\Gamma_6}^{\Gamma_6} \end{bmatrix} = \begin{bmatrix} A_1 \\ A_2 \\ A_3 \\ A_4 \\ A_5 \\ A_6 \end{bmatrix} = \begin{bmatrix} \phi^{\Gamma_1} \\ \phi^{\Gamma_2} \\ \phi^{\Gamma_3} \\ \phi^{\Gamma_4} \\ \phi^{\Gamma_5} \\ \phi^{\Gamma_6} \end{bmatrix} \quad (8b)$$

求解式(8a)或式(8b),可以获得前六阶幅值系数。由于切口前六阶奇性占主导地位,取前六阶能够达到足够高的精度。如果需要更高阶的幅值系数,可以通过继续增加结点的方式获得。

为了验证本文方法的有效性,研究不同特征半径 ρ 对幅值系数计算结果的影响,如图 7 所示,图 7 中 type(a)指取位移值用式(8a)计算的结果,type(b)指取电势值用式(8b)计算的结果。采用了图 2 三种不同密度的网格,切口尖端为每圈 5 个、10 个以及 20 个单元,分别表示粗糙、稀疏和精细网格。可以看出,提取特征半径在 0.0001 mm~0.1 mm,幅值系数计算结果不随特征半径的变化而变化,结果保持稳定;而且,当切口尖端划分为 10 个单元的稀疏网格时,结果即非常稳定,与精细的网格结果一致。取位移值计算的结果和取电势值计算的结果,也能很好得吻合。

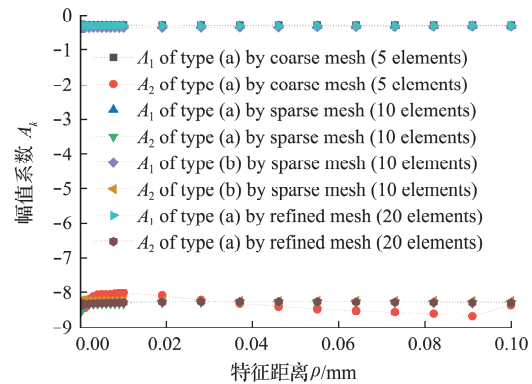
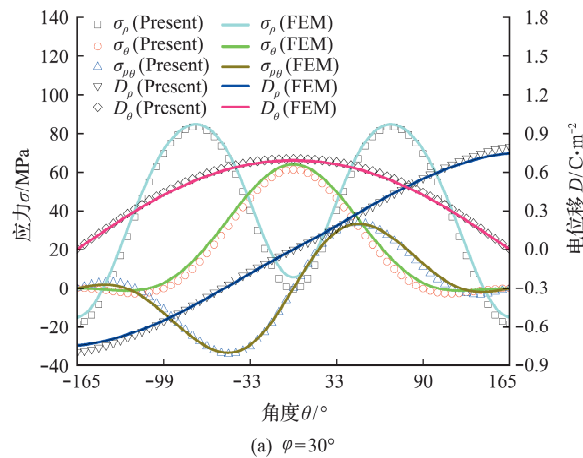


Fig. 7 特征距离对幅值系数计算结果的影响
Fig. 7 Effect of characteristic distance on the calculation results of amplitude coefficients

根据计算得到的幅值系数、奇性指数、特征角函数及其导数信息,利用式(6)重构切口尖端的奇异应力场和电位移场。计算得到的当切口角度为 30° 和 60° 时,距切口尖端半径为 0.01 mm 圆弧上的应力和电位移分布如图 8 所示,并与采用精细网

格划分的有限元计算结果对照。可以看出,本文结果与精细网格划分的有限元结果吻合,证明了本文方法的有效性,且对于两种角度的切口均适用。

图9给出了计算得到的当切口角度为 60° 时应力 σ_2 和电位移 D_2 沿 x_1 轴的变化规律,图9列出了分别取第1阶、第2阶和第3阶以及同时取前3阶

(a) $\varphi=30^\circ$

渐近展开式的计算结果。可以看出, σ_2 的主导项是第 1 阶奇性分量, D_2 的主导项是第 2 阶奇性分量, 只取前 3 阶奇性分量之和就有很高的精度, 与精细网格划分的有限元计算结果能很好吻合。

图10给出了应力强度因子和电位移强度因子随切口张角和切口深度的变化规律,可以看出,应

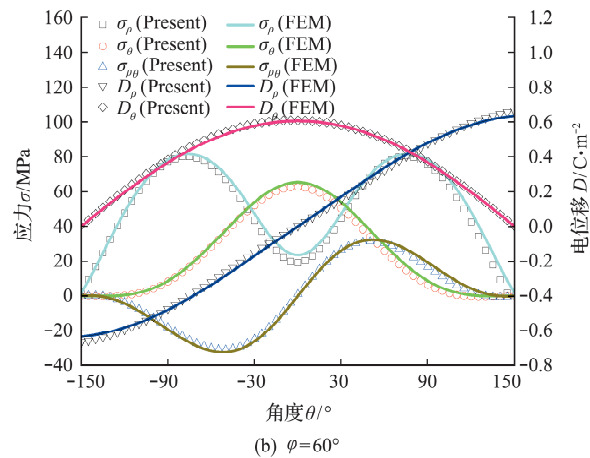
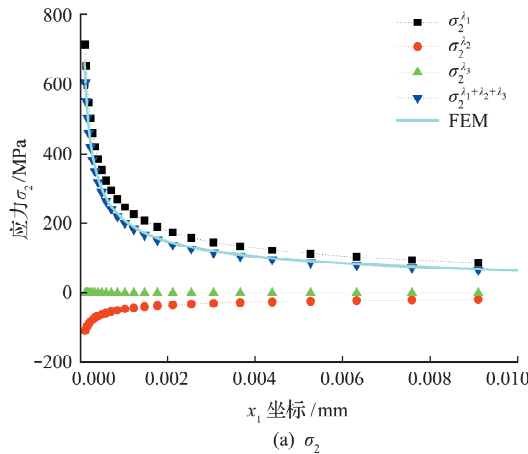
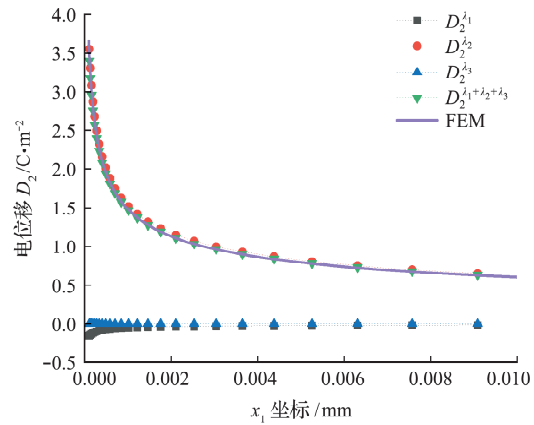
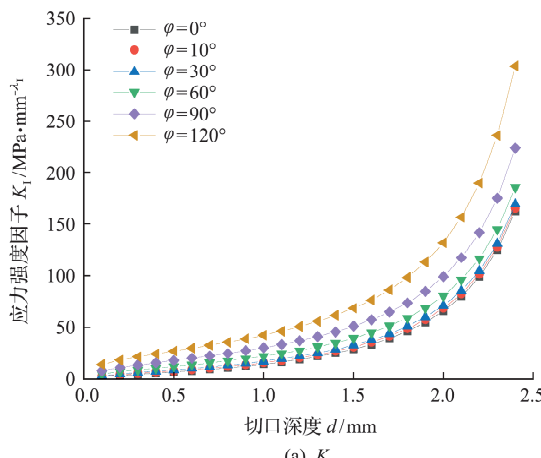
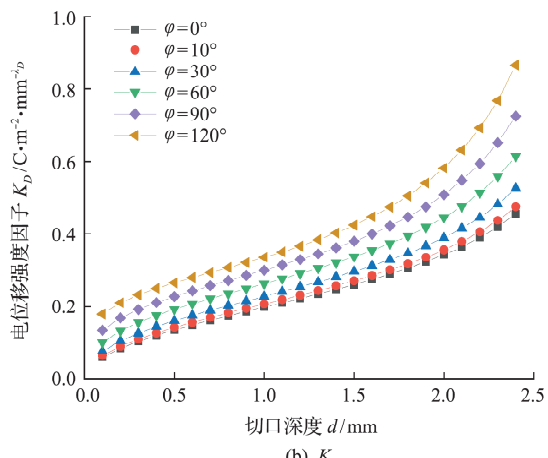
(b) $\varphi=60^\circ$

图8 半径 0.01 mm 圆弧上的应力和电位移分布

Fig. 8 Distribution of stress and electric displacement on 0.01 mm arc

(a) σ_2 (b) D_2 图9 $\varphi=60^\circ$ 时应力 σ_2 和电位移 D_2 沿 x_1 轴内点变化规律Fig. 9 Variation of σ_2 and D_2 along x_1 -axis when $\varphi=60^\circ$ (a) K_1 (b) K_D 图10 强度因子 K_1 和 K_D 随切口深度 的变化Fig. 10 Variation of intensity factors K_1 and K_D with notch depth

力强度因子随着切口深度的增加而急剧增加,电位移强度因子随着深度的增加先缓慢增加,然后才迅速增加。

5 结 论

本文利用有限元法计算得到的位移和电势较应力和电位移高一阶精度的特点,基于切口尖端奇性特征分析及位移和电势的有限元计算结果,提出了一种结合奇性特征分析和有限元法的数值方法,计算压电材料切口附近的奇异应力和电位移场。首先,将切口尖端位移和电势按渐近级数展开,推导出压电材料切口奇性特征方程并进行数值求解,获得切口奇性指数和特征角函数及其导数。再利用稀疏有限元网格计算出切口尖端附近节点的位移值和电势值,代入渐近展开式,求解出幅值系数。随后,重新利用渐近展开式,计算出切口尖端的奇异应力场和奇异电位移场。数值算例显示,本文方法受截取的特征半径影响小,计算结果稳定,利用稀疏有限元网格,能达到精细网格有限元法的计算精度。本文方法适合嵌入有限元软件,能显著提高分析压电材料切口结构尖端奇异物理场的计算效率。

参考文献(References):

- [1] Pramod A L N,Ooi E T,Song C M,et al. Numerical estimation of stress intensity factors in cracked functionally graded piezoelectric materials—A scaled boundary finite element approach [J]. *Composite Structures*, 2018, **206**:301-312.
- [2] Singh S K,Singh I V. Extended isogeometric analysis for fracture in functionally graded magneto-electro-elastic material[J]. *Engineering Fracture Mechanics*, 2021, **247**:107640.
- [3] 仲红俊,雷 钧,张传增.压电界面裂纹裂尖强度因子的显式计算公式[J].计算力学学报,2013, **30**(3):418-421,436.(ZHONG Hong-jun,LEI Jun,ZHANG Chuan-zeng. Determination of intensity factors for interfacial cracks in TIP materials[J]. *Chinese Journal of Computational Mechanics*, 2013, **30**(3): 418-421, 436. (in Chinese))
- [4] 徐 燕,杨 娟.压电压磁材料中正n边形孔边裂纹分析[J].计算力学学报,2022, **39**(6):754-760.(XU Yan,YANG Juan. Analysis of regular n -polygon hole with radial edge cracks in magneto-electro-elastic composites [J]. *Chinese Journal of Computational Mechanics*, 2022, **39**(6):754-760. (in Chinese))
- [5] Hirai H,Chiba M,Abe M,et al. Stress intensity factor analysis of an interfacial corner between piezoelectric bimaterials using the H-integral method[J]. *Engineering Fracture Mechanics*, 2012, **82**:60-72.
- [6] Hrstka M,Profant T,Kotoul M. Electro-mechanical singularities of piezoelectric bi-material notches and cracks[J]. *Engineering Fracture Mechanics*, 2019, **216**:106484.
- [7] Cheng C Z,Cheng X,Niu Z R,et al. Singularity characteristic analyses for magneto-electro-elastic V-notches[J]. *European Journal of Mechanics-A/Solids*, 2016, **57**:59-70.
- [8] Zhou Z H,Yang Z T,Xu W,et al. Evaluation of electroelastic singularity of finite-size V-notched one-dimensional hexagonal quasicrystalline bimaterials with piezoelectric effect [J]. *Theoretical and Applied Fracture Mechanics*, 2019, **100**:139-153.
- [9] 平学成,陈梦成,谢惠民,等.压电材料V型切口端部电弹性场研究[J].固体力学学报,2008, **29**(1):78-84.(PING Xue-cheng,CHEN Meng-cheng,XIE Hui-min, et al. On the electro-mechanical fields near V notches in piezoelectric ceramics[J]. *Chinese Journal of Solid Mechanics*, 2008, **29**(1):78-84. (in Chinese))
- [10] Yosibash Z,Szabo B A. A note on numerically computed eigenfunctions and generalized stress intensity factors associated with singular points[J]. *Engineering Fracture Mechanics*, 1996, **54**(4):593-595.
- [11] Niu Z R,Ge D L,Cheng C Z,et al. Evaluation of the stress singularities of plane V-notches in bonded dissimilar materials[J]. *Applied Mathematical Modelling*, 2009, **33**(3):1776-1792.
- [12] Chen M C,Ping X C,Xie H M,et al. Numerical and experimental analyses of singular electro-elastic fields around a V-shaped notch tip in piezoelectric materials [J]. *Engineering Fracture Mechanics*, 2008, **75**(18):5029-5041.
- [13] Xu X L,Rajapakse R K N D. On singularities in composite piezoelectric wedges and junctions[J]. *International Journal of Solids and Structures*, 2000, **37**(23):3253-3275.

Evaluation of singular physical field near the vertex of piezoelectric material notch

PAN Wei, CHENG Chang-zheng*, WANG Fei-yang, LI Teng-yue, NIU Zhong-rong

(School of Civil and Hydraulic Engineering, Hefei University of Technology, Hefei 230009, China)

Abstract: The idea of combining the singularity characteristic analysis with the finite element method is used to calculate the singular physical fields near the vertex of a notch of a piezoelectric material. Firstly, based on the singular asymptotic expansion technique, the singular characteristic equation of the notch is established. The interpolating matrix method is then introduced to solve it. The singularity order, characteristic angular function and its derivative of the singular asymptotic expansion are obtained. The displacement and electric potential near the notch are calculated on a relatively sparse finite element mesh. These results are introduced into the asymptotic expansion to obtain the amplitude coefficients in the asymptotic expansion. According to the calculated amplitude coefficients, singularity order, characteristic angular function and its derivative, the singular physical field can be reconstructed, and then the stress and electric displacement intensity factors can be calculated. The proposed semi-analytical method is based on the results from the finite element sparse grid. Thus, a small amount of calculation is needed and a higher-precision singular physical field can be obtained. The proposed method does not need to modify the interpolation function of the finite element method. It is suitable for embedding into the commercial finite element software.

Key words: piezoelectric material; notch; asymptotic expansion; singular stress field; singular electric displacement field

(上接第 717 页)

Meshless extended finite volume method of compositional reservoir model

RAO Xiang^{*1,2,3}, XU Yun-feng^{1,2}, LIU Wei^{1,2}, ZHOU Yu-hui^{1,2}, LIU Yi-na^{1,2}

(1. Hubei Key Laboratory of Drilling and Production Engineering for Oil and Gas, Yangtze University, Wuhan 430100, China;

2. School of Petroleum Engineering, Yangtze University (Wuhan Campus), Wuhan 430100, China;

3. Ali I. Al-Naimi Petroleum Engineering Research Center, Physical Science and Engineering Division, King Abdullah University of Science & Technology, Jeddah 23955-6900, Saudi Arabia)

Abstract: In this paper, the first meshless numerical solver of compositional reservoir models is developed. This meshless solver uses the point cloud which is subject to few topology constraints when generating and the extended finite volume method (EFVM) to discretize the reservoir calculation domain and the governing equations respectively, and can directly use the existing nonlinear solver in a mesh-based commercial simulator to calculate the global nonlinear discrete equations to obtain the profiles of pressure, phase saturation, and component concentration. In this paper, two typical compositional reservoir models (including CO₂ flooding and steam flooding) are implemented to test the computational performance of the meshless simulator. The results of the numerical examples show that compared with the mesh-based methods, the meshless simulator can significantly reduce the difficulty of discretization of the computational domain of complex reservoirs, avoid the grid orientation effect of the Cartesian grid-based (FVM), and improve the computational accuracy and convergence efficiency of the nonlinear solver.

Key words: generalized finite difference method; meshless extended finite volume method; compositional reservoir model; reservoir numerical simulation